AFRL-RV-PS-
TR-2008-1005

AFRL-RV-PS-
TR-2008-1005

Theory of Intrinsic Defects in Crystalline GeTe and of Their Role in Free Carrier Transport

Novel Materials and Device Research

Arthur Edwards

1 January 2008

Final Report

AIR FORCE RESEARCH LABORATORY
Space Vehicles Directorate
3550 Aberdeen Ave SE
AIR FORCE MATERIEL COMMAND
KIRTLAND AIR FORCE BASE, NM 87117-5776

DTIC Copy

NOTICE AND SIGNATURE PAGE

This report was cleared for public release by the Air Force Research Laboratory Space Vehicles Directorate Public Affairs Office and is available to the general public, including foreign nationals. Copies may be obtained from the Defense Technical Information Center (DTIC) (http://www.dtic.mil).

AFRL-VS-PS-TR-2008-1005 HAS BEEN REVIEWED AND IS APPROVED FOR PUBLICATION IN ACCORDANCE WITH ASSIGNED DISTRIBUTION STATEMENT.

//signed//
ARTHUR EDWARDS
Program Manager

//signed//
JOHN P. BEAUCHEMIN, Lt Col, USAF
Deputy Chief, Spacecraft Technology Division
Space Vehicles Directorate

REPORT DOCUMENTATION PAGE

Form Approved
OMB No. 0704-0188

1. REPORT DATE *(DD-MM-YYYY)*	**2. REPORT TYPE**	**3. DATES COVERED** *(From - To)*
01/01/2008	Final Report	01/10/2003 to 01/01/2008

4. TITLE AND SUBTITLE
Theory of Intrinsic Defects in Crystalline GeTe and of Their Role in Free Carrier Transport
Novel Materials and Device Research

5a. CONTRACT NUMBER

5b. GRANT NUMBER

5c. PROGRAM ELEMENT NUMBER

6. AUTHOR(S)
Arthur H. Edwards

5d. PROJECT NUMBER
2305

5e. TASK NUMBER
RP

5f. WORK UNIT NUMBER
AA

7. PERFORMING ORGANIZATION NAME(S) AND ADDRESS(ES)

Air Force Research Laboratory
Space Vehicles Directorate
3550 Aberdeen Ave., SE
Kirtland AFB, NM 87117-5776

8. PERFORMING ORGANIZATION REPORT NUMBER
AFRL-RV-PS-TR-2008-1005

9. SPONSORING / MONITORING AGENCY NAME(S) AND ADDRESS(ES)

10. SPONSOR/MONITOR'S ACRONYM(S)

11. SPONSOR/MONITOR'S REPORT NUMBER(S)

12. DISTRIBUTION / AVAILABILITY STATEMENT
Approved for public release; distribution is unlimited. (Clearance #RV08-190).

13. SUPPLEMENTARY NOTES

14. ABSTRACT

We present a study of the electronic structure and formation energies of germanium/tellurium vacancy and antisite defects in germanium telluride. We find that germanium vacancies are the most readily formed defect, independent of Fermi level. Furthermore, we find that, while the ideal crystal is predicted to be a semiconductor, the predicted large densities of germanium vacancies result in partially filled valence band and p-type conductivity.

15. SUBJECT TERMS
Chalcogenide alloys, reconfigurable electronics

16. SECURITY CLASSIFICATION OF:			**17. LIMITATION OF ABSTRACT**	**18. NUMBER OF PAGES**	**19a. NAME OF RESPONSIBLE PERSON**
a. REPORT	**b. ABSTRACT**	**c. THIS PAGE**			Arthur H. Edwards
Unclassified	Unclassified	Unclassified	Unlimited	16	**19b. TELEPHONE NUMBER** *(include area code)*

Standard Form 298 (Rev. 8-98)
Prescribed by ANSI Std. 239.18

Contents

1 Introduction

For over thirty years switching has been observed between high and low conductivity states in a variety of chalcogen-based alloys (Bahl and Chopra, 1970) (Das et al., 1987). Many chalcogenide systems switch between these two states within tens of nanoseconds when exposed to laser light or to electrical current. However, upon thermal heating, the transition can take minutes (Lu and Libera, 1995), implying that the laser- and electrically-induced phase transition depends on electronic transport. There have been several studies of the electronic structure of crystalline (Cohen et al., 1964) (Rabe and Joannopoulos, 1987) and amorphous (O'Reilly et al., 1981) (Reilly, 1982) phases. All calculations of the perfect rhombohedral material predict a band gap between 0.4 eV (Rabe and Joannopoulos, 1987) and 0.7 eV (Edwards et al., 2005). However, transport studies indicate that the polycrystalline material is metallic (Bahl and Chopra, 1970). The dominant carriers are observed to be holes.

Here, we report the first cogent theoretical explanation of the apparent contradiction between theory and the observed free-carrier transport. We used density functional theory to show that the p-type metallic character is the result of a large equilibrium concentration of the Ge vacancy. We have calculated the conformation, electronic structure, and formation energies of the vacancy and antisite defects in the low temperature, rhombohedral phase of crystalline germanium telluride (space group $R3m$). We then focus on the materials behavior induced by the germanium vacancy, by far the most easily formed intrinsic defect.

2 DFT Theory

We used QUEST, an electronic structure program based on density functional theory and using a well converged Gaussian local orbital basis (double-zeta with polarization). We used the local density approximation, the Perdew-Zunger parameterization (Perdew and Zunger, 1981) of the Ceperly-Alder free-electron exchange correlation potential (Ceperley and Alder, 1980), and Hamann pseudopotentials (Hamann, 1989). We used Monkhorst-Pack (M-P) k-grids (Monkhorst and Pack, 1976) of varying sizes for different unit cells. We show elsewhere (Edwards et al., 2005) that our results are converged with respect to k-point sampling and to numerical grid spacing. For the

defect calculations, we used three different supercell sizes containing 64, 128, and 250 atoms. The 64-atom cell was built from an 8-atom nonprimitive cell, while the 128-and 250-atom cells were built from the two-atom primitive cell. We used a 3x3x3 M-P k-grid in the two smaller unit cells, and a 2x2x2 M-P k-grid in the largest supercell. For the two larger supercells, this k-gridding is equivalent to 12x12x12 and 9x9x9 k-grids in the primitive rhombohedral cell. Because the smallest supercell was derived from a nonprimitive cell, there is no strict equivalence to gridding in the primitive cell. However, the density of k-points is greater than for a 9x9x9 gridding in the primitive cell.

We calculated the electrical levels using:

$$E(n-1/n) = E_d(n-1) + E_p(n) - E_d(n) - E_p(n-1), \tag{1}$$

where E_p (E_d) refers to the total energy of the perfect (defective) unit cell. With this definition, the reference for the electrical levels depends on the sign of the charge state(s) involved. For n-1 less than (greater than or equal to) zero the reference is the conduction (valence) band edge.

We calculated the formation energies for defects using two methods. The first is the standard relationship for highly localized defects:

$$E_{form}(q) = E_d(q) - E_p(q=0) - \sum_{i=1}^{ntype} (N_i \mu_i) + q\epsilon_F \tag{2}$$

In the second we followed an analogous prescription to Eq. 1:

$$E_{form}(q) = E_d(q) - E_p(q) - \sum_{i=1}^{ntype} (N_i \mu_i) + q\epsilon_F \tag{3}$$

where μ_i is the chemical potentials for the reservoir of type i atoms, and N_i is the number of type i atoms added to (>0) or removed from (<0) the perfect system to make the defect. Both of these prescriptions can account for different growth ambients (Laks et al., 1992). We calculated formation energies for Te-rich and Ge-rich environments and for the case where both reservoirs are available. The standard states for the Ge and Te reservoirs are the respective elemental solids. Eqs. 2 and 3 are identical for the neutral charge state. In Eq. 3, the zero of energy is given by the last occupied state in the perfect supercell. Hence, for the -/0 charge state, we have to subtract an effective band gap energy to align the formation energies. For both prescriptions, we assign the zero of energy as the energy of formation for

the stoichiometric supercell cell when the Fermi-level is at the valence band edge. For a given defect, the electrical levels and $E_{form}(q)$ at one value of the Fermi energy determine $E_{form}(q)$ for all values of the Fermi energy. Eq. 3 gives results for the charged defects that are internally consistent. That is, we can start in any charge state and derive the same formation energy as a function of Fermi energy. This is not true for Eq. 2, for which the charged results are shifted by a factor that is independent of the defect, but depends on the size of the supercell. As discussed at length elsewhere, this is the result of negligible charge localization for these defects. All energies of formation reported here were calculated using Eq. 3.

3 Results

In Fig. 1 we show the electrical levels (symbols) and the formation energies of the vacancy and antisite defects as a function of Fermi level, for a germanium-rich environment. The results are identical qualitatively and similar quantitatively for the other two cases. There are several important

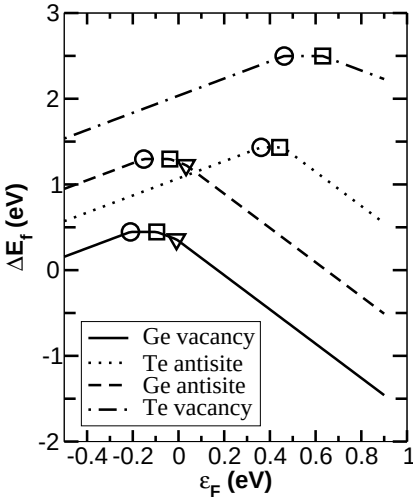

Figure 1: Calculated electrical levels (symbols) and formation energies, for germanium-rich growth, as a function of Fermi level, for the intrinsic antisite and vacancy defects. Symbols have the following meanings:◯: o/+, □:-/o, ▽:=/-. The zero of Fermi energy is at the valence band edge.

features in Fig 1. First, all four defects are predicted to have a positive U_{eff}

(Anderson, 1975). Second, for the germanium vacancy and the germanium antisite defects, the 0/+, -/0, and =/- electrical levels are all at or below the valence band edge. Third, and most important, the Ge vacancy is, by far, the most readily formed defect at any Fermi-level. While not shown here, this is independent of the growth ambient.

In Fig. 2 we show the local equilibrium structure of the ideal crystal, and of the germanium vacancy. The local geometrical parameters are given in Table 1. The crystal is made of sheets of atoms, where each atom has approximately six fold-coordination. However, three neighbors in the same sheet are slightly closer than those in the next sheet. We use the terms inter- and intra-sheet to distinguish the two sets of nearest-neighbors.

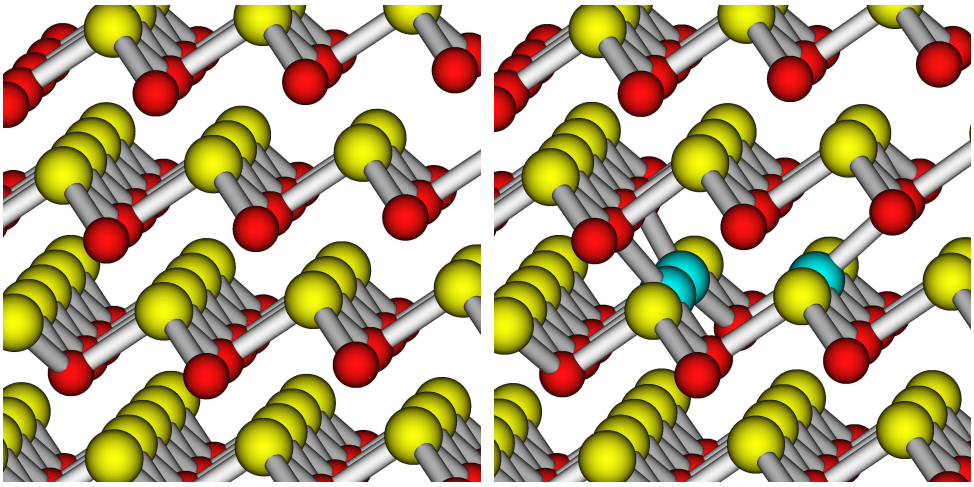

(a) (b)

Figure 2: Geometries rhombohedral GeTe (a), and the Ge vacancy (b). Red atoms are germanium, gold are tellurium. For vacancy, (b), nearest-neighbor Te atoms are blue for clarity.

The changes in both bond length and bond angle around the vacancy are small, although there is clear reconstruction. Each intrasheet, nearest-neighbor, tellurium atom bonds intersheet to one germanium atom that is directly opposite the vacancy site.

In Fig 3 we show the total density of states (TDOS) for the vacancy, superimposed on the TDOS for bulk GeTe. Remarkably, the germanium vacancy introduces no one-electron levels in the forbidden gap. To explore the

	Perfect	Ge vacancy
$R_{Te(nn)-Ge}$ (Å)	2.82	2.79
$R_{Te(nn)-Te(nn)}$ (Å)	4.15	4.08
$R_{Te(nn)-Ge'}$	3.14	(2.92,3.11)
$\angle Ge-Te(nn)-Ge(^\circ)$	94.7	93.7

Table 1: Calculated equilibrium geometries for the Germanium vacancy in rhombohedral GeTe for the 128 atom supercell. *(nn)* indicates the (intrasheet) nearest neighbors to the defect. Primed atoms indicates intersheet distances. The pair of values in parentheses indicates bonded and unbonded intersheet distances. Local geometries for the 128 and 250 atom supercells are nearly identical.

localization for the germanium vacancy, we calculated projected densities of states on the nearest-neighbor tellurium atoms and on the second nearest-neighbor germanium atoms and compare these to tellurium and germanium atoms in the bulk. There were no significant changes for the germanium atom. However, as shown in Fig. 4, there are two prominent features in the nearest-neighbor tellurium PDOS that are absent in the perfect crystal: one roughly 0.25 eV below the valence band edge and one very deep ($\sim$-15.2 eV) that is part of the Te *s*- bands. The PDOS for a Te atom roughly 10 Åaway from the vacancy is indistinguishable from the perfect crystalline case. As shown in Fig 1, the calculated V_{Ge} 0/+ electrical level is 0.21 eV *below* the valence band edge, consistent with the one electron PDOS. For all the unit cells containing one Ge vacancy, the Fermi level is *below* the valence band edge. For the neutral germanium vacancy, there is an empty state (two holes) at the top of the valence band. To understand this more fully, we integrated over the density of occupied states for the perfect and the defective super lattices. Removing the germanium atom removes one state from the valence bands, while removing four electrons, thus leaving a completely empty state at the valence band edge. Often localized defects have energy levels that depend on occupation. To explore this possibility, we added first one and then two electrons and allowed the system to relax completely. In both cases the added charge induced negligible atomic relaxations. Furthermore, we calculated the TDOS for the germanium vacancy with two electrons added to the system and used Van de Walle's method (Laks et al., 1992) to align with the eigenstates of the neutral vacancy. There is no discernible difference between these two functions. Finally, we calculated the difference in pseudocharge

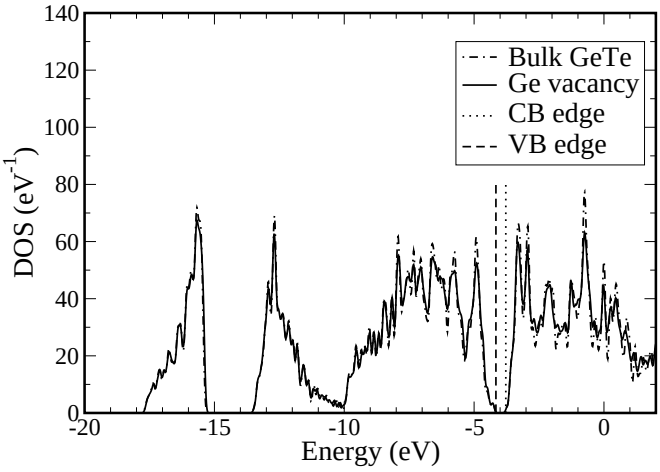

Figure 3: Total density of states (DOS) for the germanium vacancy superimposed on the DOS for bulk GeTe.

density on the nearest-neighbor germanium atoms between the neutral and -2 charge states and found it to be consistent with uniform distribution. All of these results are consistent with the extra electrons occupying valence band states that are unperturbed by the defect. Shallow levels can merge with the band edge artificially if the super cell is too small. In fact, for shallow donors and acceptors, the supercell method is inappropriate. We studied the electrical levels as a function of unit cell size and find the results reported here are qualitatively insensitive. In fact, the 0/+ electrical level for the germanium vacancy moves deeper into the valence bands for increased unit cell size. So we have the case that the defect state shows localization through the PDOS, but any added charge is purely delocalized.

Significantly, when the Fermi level is near mid-gap, as for the perfect solid, we predict that the Ge vacancy has a negative formation energy. However, a small formation energy at the valence band edge that decreases rapidly as the Fermi level moves upward from the valence band implies that the Fermi level will always be near or below the valence band edge. As discussed in detail in Ref. (Edwards et al., 2005), we calculated the Fermi level and vacancy concentrations as a function of temperature. The results are shown in Fig. 5. For all temperatures, the calculated equilibrium Fermi-level is within 0.1 eV of the valence band edge, and there is a large density of holes. For tellurium-rich growth environments, we predict equilibrium vacancy concentrations

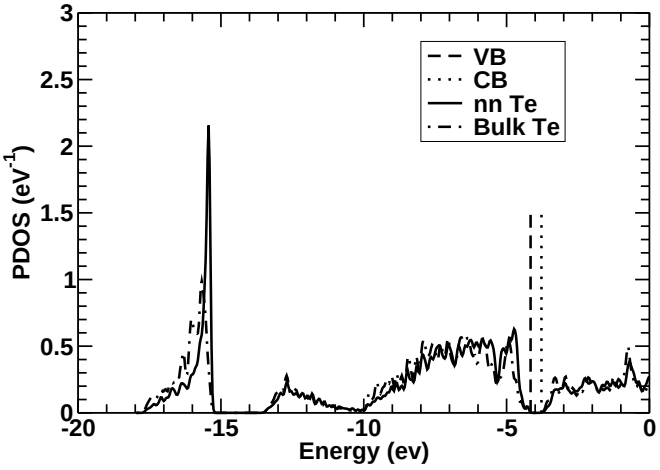

Figure 4: Comparison of projected density of states for a tellurim atom in perfect, R3m GeTe and for the nearest-neighbor tellurium atom for the germanium vacancy.

starting at 4x10^{19} cm^{-3}. This is qualitatively consistent with measurements by Bahl and Chopra (Bahl and Chopra, 1970), although they claim that the Fermi level is inside the valence band by approximately 0.3-0.5 eV. Based on our calculations, this would imply highly non-equilibrium growth conditions, or a significant overestimation of the calculated formation energy for the germanium vacancy.

4 Conclusions

To conclude, through the first systematic, first principles study of the vacancy and antisite defects in rhombohedral germanium telluride, we have shown that the electronic structure and, hence, the nature of free carrier transport is determined by the germanium vacancy. It is, by far, the most easily formed of these defects. Because of the electrical-level positions, its formation energy is monotonically decreasing with increasing Fermi levels inside the forbidden gap. Our equilibrium prediction is that the Fermi-level is just above the valence band edge, leading to hole concentrations greater than 10^{19} cm^{-3}. This gives a natural explanation for the experimental observation that germanium telluride is always p-type. It also gives a qualitative explanation

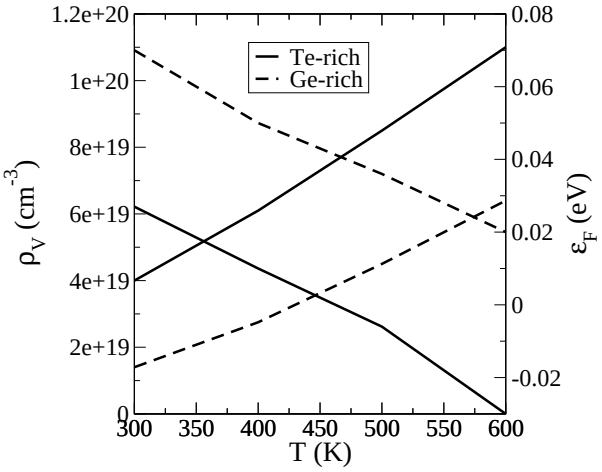

Figure 5: Calculated equilibrium vacancy concentration and Fermi-energy (w.r.t the valence band edge) as a function of temperature. Monotonically increasing (decreasing) curves are referenced to the left-hand (right-hand) y-axis.

of the origin of metallic hole conduction.

5

References

S. K. Bahl and K. L. Chopra, "Amorphous versus crystalline gete fillms iii. electrical properties and band structure," *J. Appl. Phys.*, vol. 41, no. 5, pp. 2196–2212, 1970.

V. D. Das, N. Soundararajan, and M. Pattabi, "Electrical conductivity and thermoelectric power of amorphous sb_2te_3 thin films and amorphous-crystalline transition," *Journal of Materials Science*, vol. 22, pp. 3522–28, 1987.

Q. M. Lu and M. Libera, "Microstructural measurements of amorphous gete crystallization by hot-stage optical microscopy," *J. Appl. Phys.*, vol. 77, pp. 517–521, 1995.

M. H. Cohen, L. M. Falicov, and S. Golin, "Crystal chemistry and band structures of the group v semimetals and the iv-vi semiconductors," *IBM Journal of Research and Development*, vol. 8, pp. 215–227, 1964.

K. M. Rabe and J. D. Joannopoulos, "Structural properties of gete at *T=0*," *Phys. Rev. B*, vol. 36, pp. 3319–3324, 1987.

E. P. O'Reilly, J. Robertson, and M. J. Kelly, "The structure of amorphous gese and gete," *Solid State Commun.*, vol. 38, pp. 565–8, 1981.

E. P. O. Reilly, "The electronic structure of ge-se and ge-te compounds," *J. Phys. C, Solid State Phys.*, vol. 15, pp. 1449–55, 1982.

A. H. Edwards, P. A. Schultz, A. C. Pineda, H. P. Hjalmarson, M. G. Martin, and A. P. Thompson, "Theory of self interstitials in fcc and rhombohedral germanium telluride," 2005, unpublished.

J. P. Perdew and A. Zunger, *Phys. Rev. B*, vol. 23, p. 5048, 1981.

D. M. Ceperley and B. J. Alder, *Phys. Rev. Lett.*, vol. 45, p. 566, 1980.

D. R. Hamann, "Generalized norm-conserving pseudopotentials," *Phys. Rev. B*, vol. 40, pp. 2980–2987, 1989.

H. J. Monkhorst and J. D. Pack, "Special points for brillouin-zone integrations." *Phys. Rev. B*, vol. 13, pp. 5188–92, 1976.

D. B. Laks, C. G. van de Walle, G. F. Neumark, P. E. Blöchl, and S. T. Pantelides, "Native defects and self-compensation in znse," *Phys. Rev. B*, vol. 45, pp. 10 965–10 978, 1992.

P. W. Anderson, "Negative effective u," *Phys. Rev. Lett.*, vol. 34, pp. 953–956, 1975.

DISTRIBUTION LIST

DTIC/OCP
8725 John J. Kingman Rd, Suite 0944
Ft Belvoir, VA 22060-6218 1 cy

AFRL/RVIL
Kirtland AFB, NM 87117-5776 2 cys

Official Record Copy
AFRL/RVSE/Arthur Edwards 1 cy